Innovative Approach Using Ultrasonic-assisted Laser Beam Machining for the Fabrication of Ultrasensitive Carbon Nanotubes-Based Strain Gauges

Ayub KarimzadGhavidel[1*], Mohammad Zadshakoyan[1], Gholamreza Kiani[2], Jonathan Lawrence[3], Mahmoud Moradi[4]

[1] Department of Manufacturing and Production Engineering, Faculty of Mechanical Engineering, University of Tabriz, Tabriz 5166616471, Iran

[2] Department of Organic Chemistry and Biochemistry, Faculty of Chemistry, University of Tabriz, Tabriz 5166616471, Iran

[3] School of Engineering, Arden University, Arden House, Middlemarch Park, Coventry, CV3 4FJ, UK

[4] Faculty of Arts, Science and Technology, University of Northampton, Northampton NN1 5PH, United Kingdom.

Abstract

Here, we present for the first time a novel process based on the simultaneous implementation of ultrasonic vibrations (USVs) and laser beam machining (LBM) to fabricate ultrasensitive strain gauges fabricated from polymethyl methacrylate (PMMA)/carbon nanotubes (CNTs) nanocomposites. The results clearly showed that ultrasonic-assisted laser cutting reduces the surface electrical resistance up to 2.5 kΩ, while laser cutting alone is able to reduce the surface electrical resistance down to 3 kΩ towards the best conditions. Microscopic studies confirm that USVs reduce the wrapping of PMMA chains around CNTs and intensify the mechanism of electrons transfer through tunneling by improving the dispersion degree of CNTs on the surface. It was found that the prepared sample using USVs with an 80 W laser power and the beam motion

velocity of 35 mm/s presented the best performance for detecting small strains. The sensing properties of the generated sample were characterized in the strain range of 0 to 1.2%. At 1.2% strain, the relative resistance changes were 27.04%, indicating the gauge factor is higher than 20 for the fabricated strain gauge, which is about 8 times higher than the best similar samples reported previously.

Keywords: Ultrasensitive strain gauge; Ultrasonic-assisted Laser Beam Machining; Ultrasonic vibrations; Carbon nanotubes.

1. Introduction

A strain gauge is an electrical element used to measure mechanical strains applied to objects [1]. The application range of this device is enormous in different fields such as mechanics, bioengineering, aerospace, and civil engineering [2-5]. On the other hand, the low gauge factor (GF), the complicated structure, and the brittleness of commercial semiconductor strain gauges are accounted for as the shortcomings [6-8].

Great interest has been plunged to apply the different nanoparticles to offer new materials for electronic purposes in recent years [9, 10]. There are many carbon nano-forms that are promising for practical in electronic devices [11, 12]. Extensive studies have been conducted so far to surmount the aforementioned disadvantages of traditional strain gauges by employing CNTs and graphene nanostructures [3, 13-18]; although it seems that some other nanoparticles with excellent electronic properties can also be used [19, 20]. The summary of the associated literature is tabulated in Supplementary Information (SI), **Table. S1**. Despite these attempts, a precise review of the literature shows that most of the fabricated strain gauges are not able to detect small strains [21-23]; however, some CNT-based strain gauges have been designed to sense trifling strains, but

even in these cases, the amplitude of relative resistance change ($\frac{\Delta R}{R_0}$) is trivial [8, 13, 14, 24, 25]. $\frac{\Delta R}{R_0}$ is the most important characteristic of a strain gauge, determining its sensitivity versus applied strain. This category of sensors functions based on the change of electrical resistivity of CNTs networks, which are in contact with each other [7, 21, 22, 26]. By applying the stress on strain gauges, the position and arrangement of CNTs alter in the formed 3D networks. As a result, the CNT-CNT contacts or the length of interfaces increase or decrease, thereby leading to the change of CNT-based strain gauge resistivity. This mechanism limits the application of CNT-based strain gauges to large strains, since the small applied strain amplitudes cannot reorganize the filler networks construct, and thus $\frac{\Delta R}{R_0}$ parameter is insignificant [26].

Basically, to amplify the $\frac{\Delta R}{R_0}$ ratio, the electrical resistivity of CNT-based strain gauges (R_0) should be low enough to make the measurement possible by common instruments. In the case of CNT-based strain gauges, a higher concentration of CNTs in a polymer matrix is required to reach the percolation point and thus a noticeable electrical conductivity [14, 22, 27]. Since the dispersion of a high concentration of CNTs is challenging, many researchers prefer to fabricate CNT-based strain gauge sensors by the direct coating of CNTs on a surface instead of the fabrication of CNT-based nanocomposite bulks [28-32].

To scrutinize the performance of CNT-based strain gauges, first, the electron transfer mechanisms of CNT-based nanocomposites should be identified. There are two proven hypotheses in this field [33]: (I) A high CNTs concentration creates an interconnected CNTs network, which can carry electrical charges [34, 35]. (II) Tunneling is the second well-known reason for transferring electrons, intensified by decreasing the distances between CNTs [34, 35]. If mechanism (I) is the

main factor for conduction, small strains cannot change the network resistivity significantly because a large number of disconnections or new contacts between CNTs are needed to change the resistivity [26]. On the other hand, in a structure in which tunneling is dominant, the conductivity significantly depends on the distance between CNTs [33-35]. Therefore, if the CNT-based strain gauges are fabricated in such a way that the conductivity would be under a tunneling mechanism, even applying a very small strain results in a significant change in the resistivity [36]. In the case of metal-based composite, the addition of a second phase can significantly improve the dielectric properties of the resulting composite material, affecting the tunneling phenomena in this material [37, 38]; but there are two essential challenges to highlight the role of the tunneling effect in the conductivity of polymeric CNTs-based nanocomposites: (I) The CNTs should not be broken during the dispersion process to maintain CNTs distances at the least amounts [39-41]. (II) The concentration of CNTs in the polymer matrix should not be high to form CNTs networks [39, 40, 42]. Recently a method has been developed for the CNTs dispersion, entitled electrically dispersion technique (EMDT), which can protect CNTs against breakage during the dispersion process [43]. Therefore, the utilization of EMDT can assist in dominating the first challenge. To overcome the second challenge, another technique has been presented, causing a decrease in the surface's resistivity of CNTs-based nanocomposites at low concentrations [44-46]. In this method, to generate the conductive network, after the fabrication of nanocomposites at low concentrations, which are far lower than the percolation threshold, their surfaces are treated by laser beam machining (LBM).

To the best of our knowledge, there is still no method for producing ultra-sensitive and low-cost CNT-based strain gauges with a high gauge factor. To this end, we report for the first time the development of a technique for constructing a highly sensitive CNT-based strain gauge for

measuring small-magnitude strains by an innovative two-step-process approach. In the first step, a CNT-based nanocomposite is fabricated by EMDT at low concentrations, far below the percolation threshold, where CNTs are protected against fracture. In the second step, by simultaneous application of LBM and ultrasonic vibration, the surface of the nanocomposite obtained from the EMDT is treated. This procedure creates a layer on the surface of the fabricated nanocomposite that is conductive and sensitive to very low-magnitude strains.

2. Experimental details

2.1. Materials and Sample Preparation

Multi-walled CNTs (MWCNTs-NC7000) were supplied by Nanocyl SA., Belgium, and used as conductive fillers, synthesized by chemical vapor deposition (CVD). There are some other methods for the synthesis of nano-sized particles, but CNTs are commonly produced by this method [47-51]. To remove the impurity of the MWCNTs and their treatment, the explained procedure in ref [52] and [43] was followed, respectively. PMMA pellets (CM205) were purchased from CHI MEI Corporation (Taiwan). To prepare the CNT/PMMA nanocomposites, 0.24 g PMMA granules were dissolved in 2.4 mL chloroform (Sigma Aldrich, ACS. ISO. Reag. PhEur. ≥ 99.8%) at room temperature using a magnetic stirrer. Then, 2.8 mg MWCNTs were dispersed in the first mixture using the EMDT method as described elsewhere [43]. The prepared nano-suspension was converted to the solid fibers by gradual dripping in 50 mL ethanol (Sigma Aldrich, 99.6% purity) under stirring to keep the MWCNTs-based suspension homogeneous and avoid the formation of agglomerations [53-55]. This procedure was continued to collect 20 g PMMA/MWCNTs. Afterward, the collected nanocomposite fibers containing 0.2 wt.% MWCNTs were washed several times with distilled water and dried at 60 °C for 24 h. The compression molding process was used to make rectangular sheets from the prepared fibers. This operation was

carried out for 10 min under 50 bar pressure at 200 °C by an integrated mold containing 20 rectangular-shaped cavities with 1 × 1 × 30 mm dimensions. The conductivity of the compression-molded samples was measured by a Megger insulation tester BM5200, which was higher than 10^9 Ω.cm, proving that the percolation threshold did not occur. The FE-SEM (field-emission scanning electron microscopy) micrographs of different cross-sections of the fabricated samples are provided in SI, **Fig. S1**.

2.2. Laser beam machining/ultrasonic vibrations processes

The CO_2 Sahand plastic laser cutting and engraving machine with the maximum safe power of 120 W was used in this research. To provide USVs, an auto-tuned Alpha ultrasonic power supply with an adjustable frequency range from 15 up to 35 kHz and maximum output power of 2 kW, equipped with a 2 kW Branson ultrasonic transducer, was employed. A cylindrical ultrasonic horn with a center hole of 20 mm and an outside diameter of 50 mm was assembled on the transducer. The power, frequency, and amplitude of USVs were adjusted at 100 W, 18.8 kHz, and 5 µm, respectively. The prepared samples were glued directly on the horn with instant glue (SUPERUNIX).

The full factorial experimental design method was employed to study the influence of LBM variables. Herein, there are many well-known parameters such as the laser source types, power, cutting velocity, the pressure of covering gas, and focal point, which can be effective [54, 56, 57]. Investigations among these factors showed that the power and cutting velocity parameters are more effective than others [44]. Thus, in this research, the laser power (*P*) and also the cutting velocity (*V*) were selected at three levels of 50, 65, and 80 W, and 20, 27.5, and 35 mm/s, respectively. Low-pressure argon gas (0.28 MPa) was used as covering gas during all experiments. The focal point of the beam was adjusted 5 mm above the sample.

The designed experiments were conducted without (type-A) and by applying the vibration (type-B) to determine the effects of USVs, and all runs were replicated three times. The experimental layout and primary results are tabulated in **Table. S2**, indicating that the design includes 18 experiments. A direct path was cut along the 10 mm edge of each sample and divided into two equal parts. Then, the sample with a thickness of 1 mm, including the treated surface, was cut from the main part by laser, without applying USVs, at P=50 W and V=30 mm/s to decrease undesirable laser effects. The sample preparation methods and LBM/USVs operation are schematically summarized in **Fig. 1**. **Movie S1** in SI depicts the LBM/USVs process.

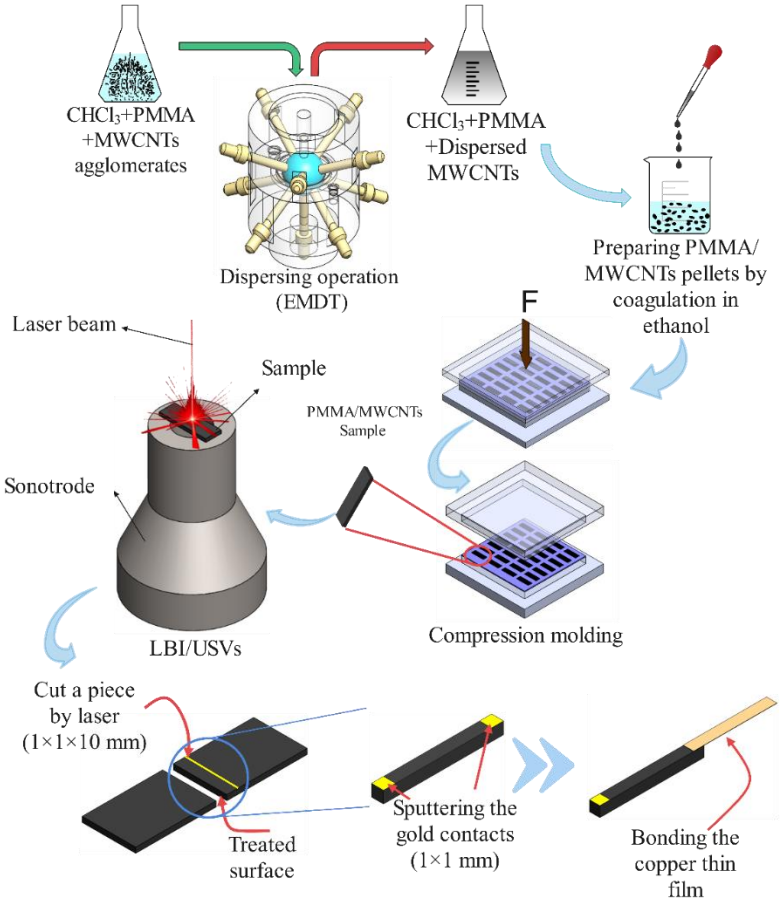

Figure 1. A schematic summary of the employed methods and the order of the procedure to fabricate ultrasensitive CNT-based strain gauges.

2.3. Techniques and methods

The morphological features of PMMA/CNTs nanocomposite samples before and after LBM/USVs processes were studied by FE-SEM (TESCAN-Mira3). To analyze, the chemical composition of the samples, energy dispersive X-ray (EDX) was carried out using the same device, and Fourier transforms infrared analysis (FTIR-Brucker-TENSOR 27). Image J software was utilized to analyze the captured micrographs. The electrical conductivity of samples was measured *via* a four-pin mode multi-meter (Agilent 3458A) with a resolution of $8\frac{1}{2}$ a digit. The current-voltage (I-V) characteristic curves were also acquired by the same multi-meter. To remove the effect of contact position and have an accurate conductivity measurement, an area of 1×1 mm on both sides of the treated surface was coated with a thin layer of gold. A copper-thin film with a thickness of 30 μm has adhered to one of the coated sites by an electrically conductive nickel-filled epoxy adhesive. The free sides of the samples were sandwiched between two sticks of the pure PCB (printed circuit board) like a cantilever beam, so the gold-coated part was in contact with the copper layer of the PCB.

Subsequently, to determine the electrical and electro-mechanical sensory properties of the samples, a set value of strain was applied from the free side of the specimen using a motorized spherometer, generating the displacement with the precision of 1 μm. Electrical resistivity was recorded at the same time when the strain was applied. Amplitudes of the strain ranged from 0 up to 1.2%. The optimized sample was determined based on electromechanical characteristics such as sensor response under alternative loads, the accuracy of function after a long working time, and response rise time. In these analyses, a data acquisition device was fabricated by programming an Arduino-UNO-Nano microcontroller board, whereas the motorized spherometer was also controlled

synchronously for this purpose. **Fig. S2** depicts the above-described setups, and **Movie S2** portrays the performance of the prepared CNT-based strain gauges.

3. Results and Discussion

3.1. Microscopic Analysis

After the incident laser beam over the surface of the nanocomposites, a major part of the polymer matrix is destructed and sublimated from the treated location [58]. **Fig. 2** shows the FE-SEM micrographs of some of the samples after the LBM treatment. The external layer of this surface, which is in direct contact with the laser beam, is first transformed to a viscous state and then re-solidified. In this boundary layer, because of the degradation of the polymer matrix, the CNTs concentration is increased extremely, thus the percolation threshold occurred, providing the electrons transport possibility [44]. However, it should be noted that some studies reported that the generated conductivity is attributed to the CNTs network formation on the processed surface [44, 59]. More micrographs are presented in **Figs. S3-S5**.

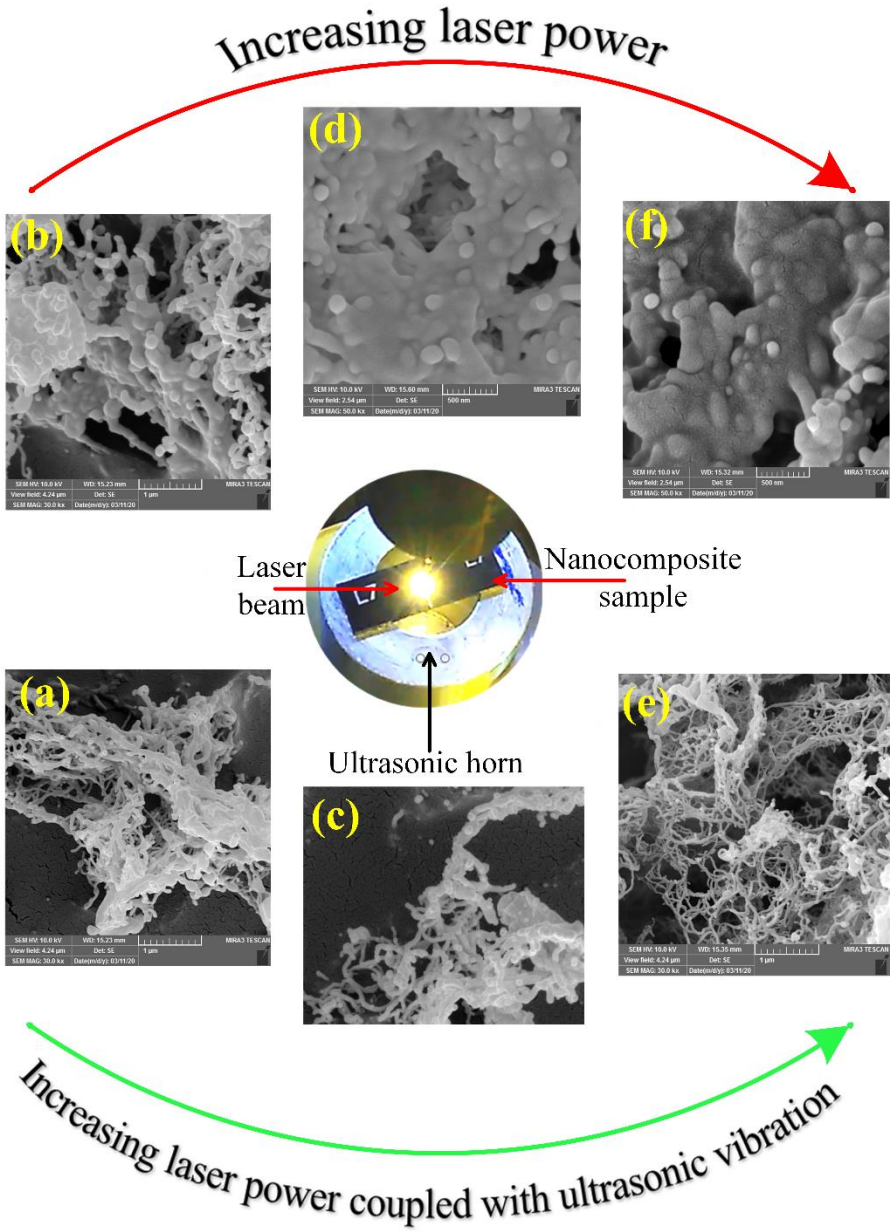

Figure 2. The effect of LBM and LBM/USVs on the morphology of samples. The images of the upper and lower rows are related to the samples treated by LBM and LBM/USVs processes, respectively. The cutting velocity in all depicted micrographs is constant, equal to 20 mm/min, and the power of the beam is (a) and (b) *P*= 50 W (c) and (d) *P*= 65 W and (e) and (f) *P*= 80 W.

According to the FE-SEM images (**Fig. 2**), most of the CNTs have appeared in the form of agglomerations on the external layers of the prepared samples without the USVs treatment. This observation confirms that the conductivity enhancement in these samples occurs only on the external surface. Therefore, its stability against environmental factors is weak, and any physical contact can disrupt the arrangement of the formed CNTs network. Thus, it is feasible that the conductivity was destroyed completely or changed substantially. For most of the samples, CNTs were wrapped by PMMA chains counted as an insulator, having undesirable effects on making influential electrical contacts. It was observed from **Fig. S3-S5** that the covering of CNTs and their agglomerates by PMMA chains was thicker at the velocity of 20 mm/s. This level of velocity by increasing the contact time of the beam with the treated surface leads to more viscosity reduction on the molten layers of the surface [58, 60, 61]. This results in more concealing of CNTs by PMMA chains [33]. At this velocity, an increase in the power leads to the same effects, thickening the coverage of CNTs accordingly. The speeding-up beam motion up to 27.5 mm/s decreased the CNTs wrapping; however, at this level of velocity, an increase in the power augments the wrapping. Subsequently, the density and thickness of PMMA chains dropped around CNTs at the velocity of 35 mm/s noticeably because the reduction in the viscosity of the boundary layer was not enough to be responsible for drastic CNTs burying. However, the power increment from 65 to 80 W reached back the previous conditions and made the coating thicker.

In the fabricated samples using the LBM/USVs processes, different phenomena such as unwrapping of PMMA chains and reduction of agglomerates' size were observed. In these samples, at a velocity up to 27.5 mm/s, the morphology of treated surfaces was approximately the same as the LBM's samples; but the coverage of CNTs is dominated by the power decrement. These observations indicated that the application of the USVs plays a positive role in wiping out

the polymer layers from the surrounding of CNTs. Another notable point about the USVs application was the coating of formed CNTs network with PMMA layers, which can empower the stability of generated conductivity against environmental threats. Nonetheless, the distribution and development of CNTs have been limited at low power levels due to the higher viscosity of boundary layers like ones made under no USVs process. But higher power utilization was successful in making a proper CNTs dispersion degree and distribution above and inside the treated surfaces.

The number of individual CNTs above and inside the processed layers was another effective parameter of the electrical conductivity. More individual CNTs raise the chance of the CNT-CNT contacts and amplify the metallic conduction [59]. Even if there is no direct contact, the charge transport possibility by the tunneling phenomenon was increased strongly due to the reduction of distances between CNTs. According to our microscopic investigations, more individual CNTs were observed on the LBM/USVs processed samples. Since FE-SEM micrographs were not able to show CNTs in the depth layers, exact quantitative amounts cannot be reported. Therefore, the ratio of observed individual CNTs to the studied area (I_N) as well as values of the ratio between holes area to studied area (H_A) was calculated and reported in **Table. S3**. In fact, thermo-dynamical transformations can form these holes by solidification of the viscous layer and its shrinking [61, 62]. Results showed that the use of the USVs decreases the H_A ratio significantly because the ultrasonic vibration hinders the boundary layer from randomly and asymmetrically shrinkages. The decomposed parts of PMMA chains (D_P) adhered on the treated surface is another microscopic observation that is reported in **Table. S3**. In this case, the USVs application reduces the number and volume of D_P, hindering the adhesion of D_P on the surface in a viscous state. The average area of agglomerates per area of 1.6 mm^2 (A_a), acquired from 10 FE-SEM micrographs for different

states of experiments, is reported in **Table. S3**. A decrease in A_a implies proper dispersion, resulting in the CNTs distance reduction, elimination of their agglomerates, and enhancement of tunneling effects. A_a results confirm that the USVs limits the formation of CNTs re-agglomerations.

The alteration of the chemical composition of the post-processed layer due to the parameters as such oxygen stoichiometry or appearing a new functional group may lead to a decrease in resistivity, which its probability of happening was investigated by EDX and FTIR [63, 64]. In EDX analysis, the interaction between the electrons and surface occurred (**Fig. S6**), causing to destruct of the surface, so the obtained results were unreliable and not reported; although the results of FTIR spectroscopy (**Fig. S7**) also confirmed no change in chemical composition except for the break of C-C interaction between the carbon nanotubes and the base polymer, formed during the nanocomposite preparation process (**Fig. S8**) [65, 66]. Therefore, to achieve a conductive layer on the interface of nanocomposite and laser beam after treatment, at least one of the following factors is required: (I) The concentration of CNTs in this layer should be surpassed the percolation threshold value, and a CNTs network should be formed (internal network) to maximize CNT-CNT contacts (metallic conduction) [67, 68]. (II) A portion of individual CNTs and their agglomerates should be present on the external surface of layers without polymer chains wrapping to make connections with the buried CNT networks. If the density of distributed CNTs is high on the surface (external network), electron transmission via the surficial network without intervening in the internal network is possible [35, 67, 69]. (III) If the dispersion degree of CNTs and their agglomerates within the internal or external network is good, it reduces the distance between conductive points and subsequently amplifies the tunneling effects [33, 70, 71].

FE-SEM analysis revealed that for type-A samples, factors (I) and (II) correspond for the surface conductivity improvement. However, it should be noted that the internal network has not been observed for these samples; therefore, the conductivity by the factor (II) occurs only on the external surface, where PMMA chains wrapping plays the key role. For type-B samples, all three mentioned factors are contributed.

The total area of agglomerate points (S_{agg}) per their number (N) is presented in **Fig. 3**. Higher values of this ratio imply the distribution of a small number of big agglomerations, indicating the distance between CNTs and their agglomerations increases while the possibility of tunneling decreases. [22, 33]. On the other hand, small ratios augment the tunneling phenomenon; nevertheless, excessive decrement of S_{agg}/N leads to diminishing the size of secondary agglomerates (that act as the electron junctions), causing a higher electrical resistivity [33]. Indeed, here S_{agg}/N plays the role of grain size in the metal-based composites which is a determinative factor in the electrical properties [72, 73]. Therefore, there is an optimum value for S_{agg}/N to reach a high conductivity.

By simultaneous investigation of obtained results for S_{agg}/N and the surface electrical resistivity, it seems that this optimum value was obtained for type-B samples, prepared by P=80 W and V=35 mm/s. The adjustment of mentioned factors changes the viscosity of the layer and does not limit either the formation of agglomerations or allow their excessive growth. A higher or lower value for the optimum S_{agg}/N, depicted in **Fig. 3** increases the electrical resistivity. In the case of the type-A sample, due to the coverage of agglomerations with PMMA chains, the influence of S_{agg}/N on the resistivity cannot be discussed because the possibility of electron transmission by tunneling was weakened [33]. Moreover, the CNTs coverage observed attenuates the effective connection by an external voltage source, decreasing the accuracy and the repeatability of resistivity

measurement [35, 74]. In these samples, the bundles or individual CNTs create the connection bridge between agglomerates, undertaking to form chiefly the conductive network [33].

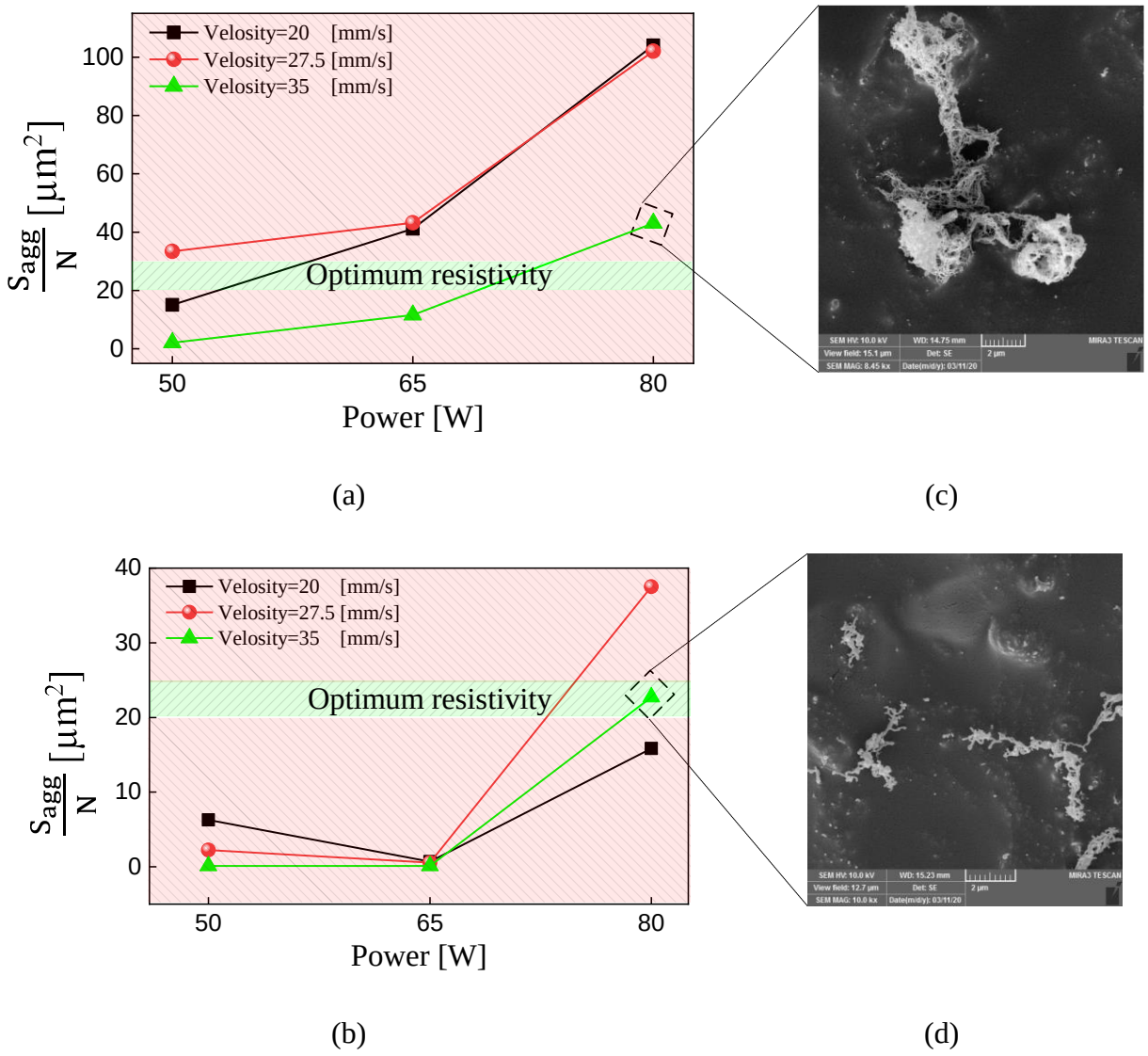

Figure 3. The influence of process variables on the relative agglomerations area S_{agg}/N [µm^2] for type-A (a) and type-B samples (b). FE-SEM images of the surface after LBM/USVs processes were prepared at *P*= 80 W and *V*=35 mm/s ((c) and (d)).

3.2. Electrical resistivity of treated surfaces

The electrical resistivity of surfaces (R_S) was reported for type-A and type-B samples in **Fig. 4(a)** and **(b)**, respectively. As can be seen, for two groups of samples, the treatment processes could significantly reduce the R_S. The comparison between the results of the literature and current findings proves that the preparation of samples using EMDT leads to higher electrical conductivity at low CNTs concentrations after the LBM process. The protection of CNTs' length in EMDT is the only reason to justify these results [44, 46, 75-79]. **Fig. 4(a)** shows that at V= 20 and 27.5 mm/s, R_S decreased gradually by increasing the power. The viscosity of polymers at temperatures higher than glass transition (T_g) is a function of temperature, usually decreasing as temperature rises [80, 81]. In the interface of laser beam and samples, the mechanical behavior of material converts from viscoelastic to viscous, where it congeals after the process and transforms into its intrinsic state [58, 60-62]. Higher laser power increases the exerted heat to the sample, and subsequently causes lower viscosity of this layer [58, 61, 82]. On the other hand, the viscosity of this layer has a substantial role on R_S, because the polymer chains can easily wrap around the CNTs in lower viscosities, acting as an insulator, intercepting the transferring of electrons [33]. As illustrated in **Fig. 4(a)**, by the increment of V from 20 up to 27.5 mm/s at a constant laser power the R_S decreases. Based on the above-mentioned interpretations, the influence of boundary layer viscosity on R_S can justify this finding. Accelerating the beam movement has a significant effect on decreasing the transferred heat to this layer, and subsequently, its viscosity [58, 60, 61], while it is more influential than the effects of the laser's power on the viscosity [61, 62]. Thus, by increasing the velocity and formation of a more viscous layer, the condition becomes more complicated to wrap PMMA chains around the CNTs, causing better conditions to benefit from the R_S reduction.

Entirely, different behaviors were observed by increasing *V* from 27.5 to 35 mm/s. At this level of velocity and *P*=50 W, a significant conductivity was expected; on the contrary, the resistance drastically increased, while the higher powers reduced R_S at an intense rate. At *V*= 35 mm/s followed by *P*=50 W, the minimum temperature of the specimen was observed compared to those of other studies under specific conditions [44, 58, 60]. Consequently, the viscosity of the layer reached the maximum possible amount. As the lower viscosities lead to an easier wrapping of CNTs, its higher values also restrict their full removal. An increase in the power up to 60 and then 80 W solves this problem by reducing the viscosity and facilitating the diminution of CNTs wrapping by PMMA chains. The microscopic findings confirmed the aforementioned interpretations and results. It can be concluded that the highest conductivity without applying the USVs can be reached by adjusting *V*=27.5 mm/s and *P*=50 W. However, it should be noted that in the laser process, the velocity of the beam should be set at the maximum amount to reduce its undesirable effects such as the development of the heat affected zones and destroying the surface texture, creation of the shrunken holes and cavities [58, 60-62, 83-85]. In other words, if it is possible to make the surface conductive by a slight reduction in the viscosity in the boundary layer, fewer unwanted laser beam incident effects are observed.

Fig. 4(b) presents the R_S of type-B samples. In terms of velocity effects, a similar trend was observed for fabricated samples without the USVs. Therefore, all conducted analyses on type-A samples (**Fig. 4(a)**) are correct. However, there are conflicting behaviors about the powerful effects at *V*=20 and 27.5 mm/s. Herein, the utilization of the USVs reduces R_S by raising the power. The reason behind this finding can be attributed to the following two occurrences: (I) By increasing the power and decreasing the viscosity and applying USVs at the same time, the PMMA chains are not able to wrap CNTs and consequently, better results for the electrical conductivity are

achieved [33, 86]. (II) The use of USVs increased the number of individual CNTs on the surface and reduced the size of the secondary agglomerates. Moreover, improving the dispersion degree empowered the tunneling mechanism [33, 87].

At V=35 mm/s, the same downward trend was observed for the R_S with an increase in power. But the slope of the graph was higher than those of other velocities. According to the microscopic observations, at this velocity and P=50 W, free CNTs were rarely observed on the surface because these levels of parameters were not able to reduce the viscosity to such an extent to form the necessary network for the conduction. An increase in the power up to 65 W, largely solved this problem, but compared to type-A samples, higher resistance was obtained. In fact, the application of USVs in medium viscosity improved the dispersion of CNTs and their wrapping by PMMA chains and reduced the electrical conductivity. Finally, by increasing the power up to 80 W, favorable conditions were created, in which a layer with a high concentration of CNTs and desired numbers of CNTs agglomerations as well as individual CNTs were obtained on the treated surfaces and its underlying layers. In these conditions (P=80 W and V= 35 mm/s), the viscosity is high enough to disperse the individual CNTs and have small agglomerates in the boundary layer. Secondly, a portion of CNTs remains unwrapped, providing the feasibility to make effective connections for electron transmission. Finally, it can be concluded that a P=80 W, V=35 mm/s, and the application of the USVs are required to obtain the minimum R_S.

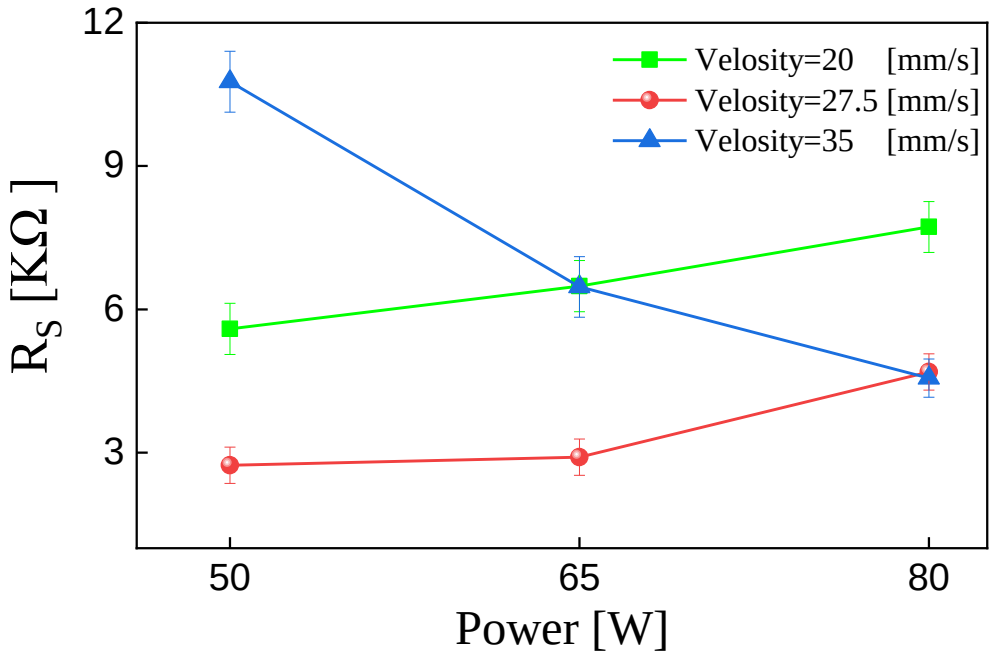

(a)

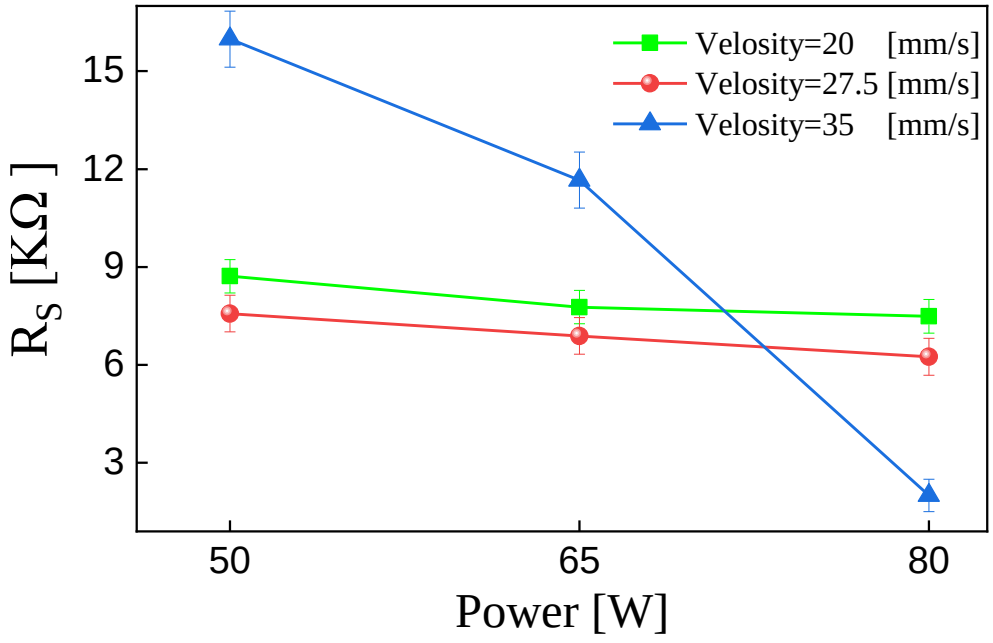

(b)

Figure 4. The effect of LBM/USVs processes variables on the surface electrical resistivity (R_S) without (a) and with (b) applying USVs.

3.3. Strain sensory properties of PMMA/CNTs samples

To detect accurately the electron transfer mechanisms in fabricated samples, their voltage-current curves (**Fig. 5)** were obtained individually by applying a series of voltages to each sample and recording the corresponding currents. The linearity of this curve implies that the electron transmission is carried out via the dominant mechanism of CNT-CNT contacts (metallic conduction), while the noticeable role of the tunneling transmission mechanism is inferred from the exponential shape of these curves [36, 88]. As shown in **Fig. 5**, for specimens without USVs, the curve is completely linear, but for fabricated samples with the USVs, the curve shows an exponential trend. Therefore, the use of the USVs causes electron transmission following the tunneling phenomenon in this layer due to the change in the structure and distribution pattern of CNTs in the surface layer and the reduction of the number of agglomerates and the distances between them. Concerning type-A samples, the formation of a CNTs network or their agglomerations on the surface is responsible for higher electrical conductivity. Results of the strain sensory analysis are also confirmed by microscopic findings and observations.

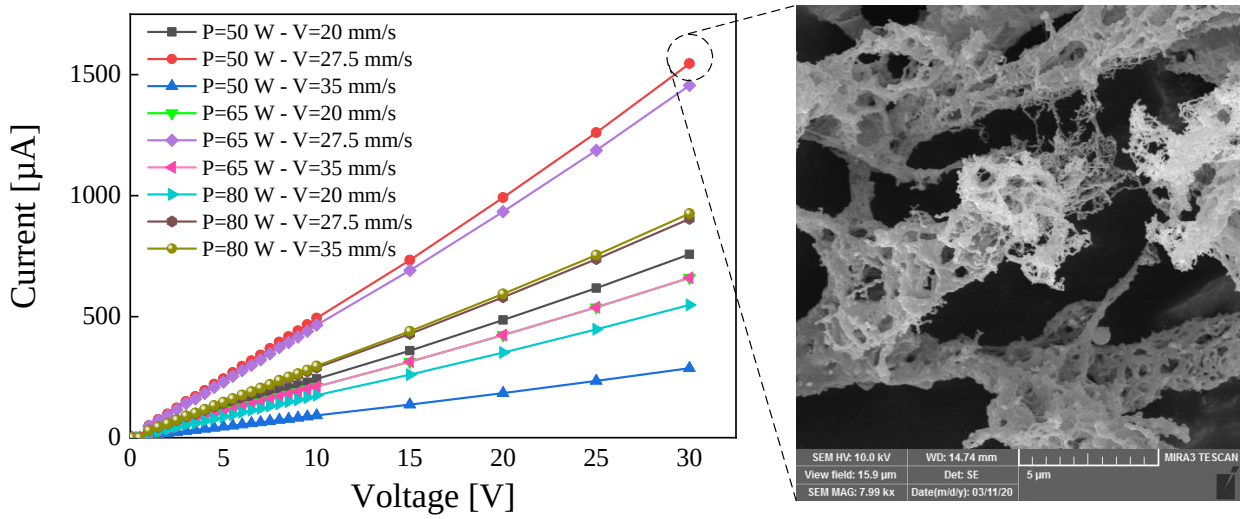

(a) (b)

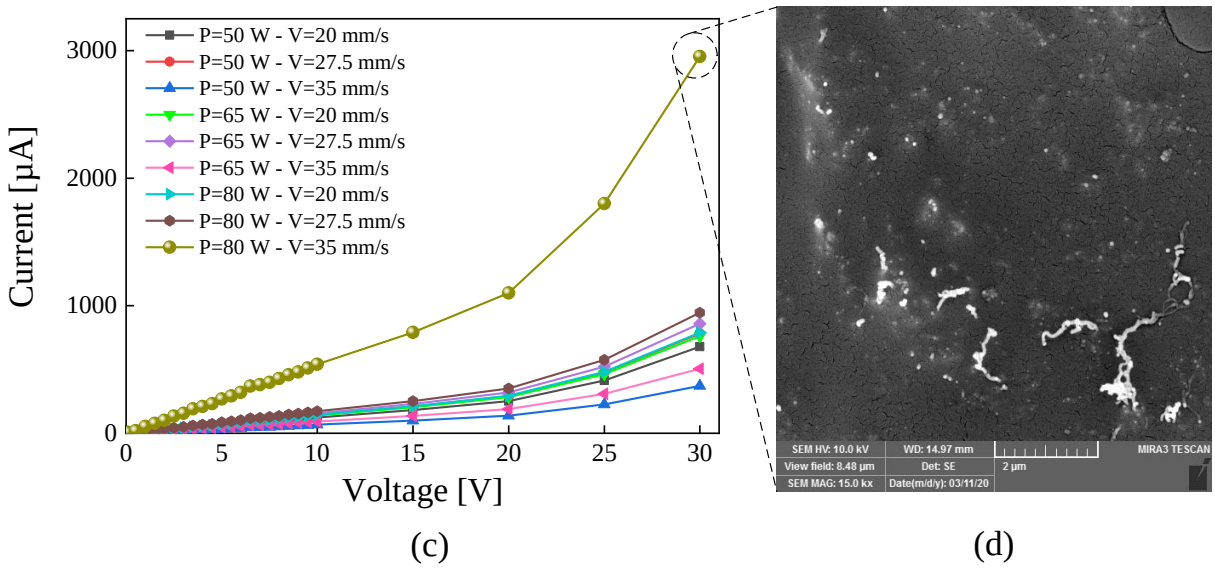

(c) (d)

Figure 5. The voltage-current curves of samples without ((a) and (b)) and with ((c) and (d)) the application of the USVs. FE-SEM images of the surface after LBM/USVs processes prepared at *P*= 50 W and *V*=27.5 mm/s (b) and *P*= 80 W and *V*=35 mm/s (d).

Preliminary experiments showed that the R_S in the samples undergoes fundamental changes by applying very small strains. If these changes are stable and repeatable, the described method in this paper can be used to fabricate ultrasensitive strain gauge sensors. For a more detailed study, the relative change of the resistance ($\frac{\Delta R}{R_0}$) were measured by applying strain in the range of 0 to 1.2 % (**Fig. 6**). It is obvious in **Fig. 6** that by applying the strain, the resistivity of both types of fabricated samples is altered. According to the microscopic investigations, the mechanism of the resistance alteration in samples without the USVs is similar to previously studied sensors, which is mainly the disconnection between CNTs or rearrangement of the CNTs network [28, 36, 89, 90]. For type-A samples, the slope changes of the diagram (**Fig. 6(a)**) are not significant by increasing the applied strain compared to the fabricated samples with the USVs, suggesting that the sensitivity of these types of samples is lower than the type-B ones. This result proves that the

USVs had not only positive effects on the R_S but also were able to improve the sensor sensitivity of the surface.

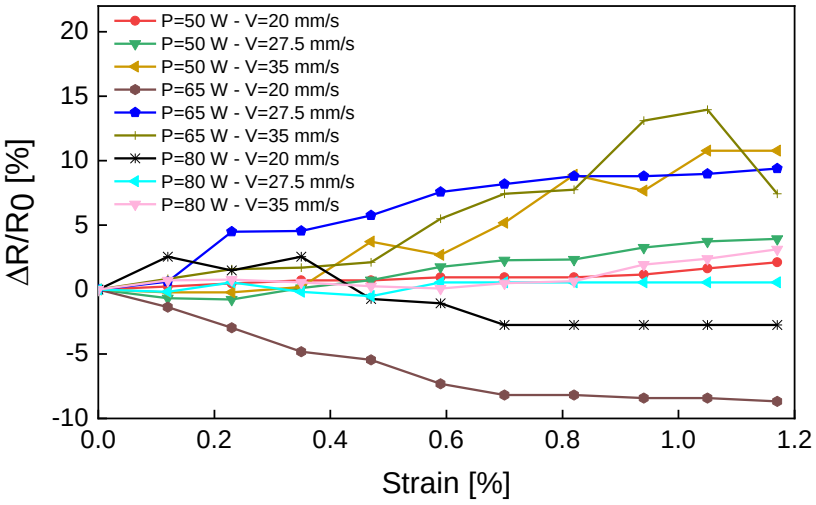

(a)

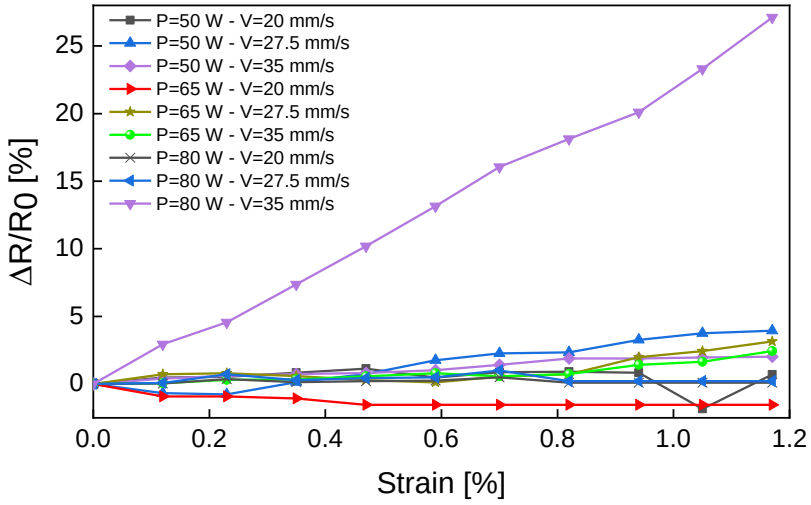

(b)

Figure 6. The strain sensing performance of samples. Relative resistance change for type-A (a) and type-B (b) samples.

Fig. 6(b) clearly portrays that the curve related to the fabricated sample in the presence of the USVs at P=80 W and V=35 mm/s shows a steep upward trend, which is almost linear. This proves that this sensor has the highest sensitivity among others. The results of electromechanical

evaluations of this specimen as a function of the strain gauge are illustrated in **Fig. 7**. **Fig. 7(a)** presents $\frac{\Delta R}{R_0}$ values of this sensor as a function of strain in bending and compressive modes. The value of $\frac{\Delta R}{R_0}$ for this sample is 27 % at 1.2 % of the tensile strain, which is about 20 and 8 times higher than the similar CNT-based sensors reported in [17] and [22], respectively. According to FE-SEM assessments, the electrical resistivity in tunneling is strongly impressed by the distances between CNTs and their agglomerates, separated by the PMMA barrier. Subsequently, applying tensile or compressive load changes these distances and increases or decreases the $\frac{\Delta R}{R_0}$ factor, respectively. This distance plays a vital role in the electron transferring phenomenon by tunneling mechanism [36, 91]. This distance grows under the effects of the bending tensions, that rise R_S. Compressive strain also leads to easier electrons transferring by bridging the conductive islands of CNTs or their bundles closer together and reducing the secondary resistance of the surface. The slope of the curves in the compressive mode is greater than in the tensile mode. In fact, an exponential relationship between the resistance and thickness of the PMMA barrier can be established by tunneling, separating two corresponding conductor regions [33, 36, 92, 93]. This physical occurrence is obvious in **Fig. 7(a)**. According to this figure, there is no residual resistance after unloading the sensor and the initial resistance of the sensor is recovered; because the resistance change is not due to the disconnection of the CNTs or CNTs network rearrangement. On the other hand, the intrinsic performance of the sensor based on the tunneling phenomenon makes it sensitive to the smallest strains, allowing sensing very small strains. The achievement of this structure is due to the application of the USVs, bringing an advantage for the proposed fabrication method in this research. The gauge factor, obtained by dividing $\frac{\Delta R}{R_0}$ to the applied strain ($G = \frac{\Delta R}{\varepsilon R_0}$) is calculated for different tensile strains, shown in **Fig. 7(b)**. For all assessed strains, the

obtained *GF* was higher than 20, which is 10 times higher than those of the available commercial strain gauges [94, 95]. One of the fundamental characteristics of strain gauges is the stability of their electrical resistance alteration by applying different strains over time. **Fig. 7(c)** shows the ratio of instantaneous ΔR to average ΔR under three different tensile strains over 300 s. As can be seen in **Fig. 7(c)**, in the most unstable conditions, these changes fluctuate in the range of less than -0.1 to +0.3, implying a good accuracy in terms of output stability. Moreover, **Fig. 7(f)** demonstrates the performance of the sensor upon applying periodic strains after 1 s and 1, 4, and 12 h at frequency of 1 Hz and strain (ε) range of 0 to 1%. The results of this evaluation can be considered as a factor to identify the strength and durability of the sensor. In **Fig. 7(f)**, after a long time (≈12 hr) use of the sensor, its initial resistance increases insignificantly. Obviously, under a long-term periodic loading, the stress relaxation occurred in the PMMA matrix [96, 97], leading to the separation of conductive points. This phenomenon increases the resistivity of the unloading state [13, 26, 28, 98] and weakens the conduction caused by the tunneling [33, 99]. At small strains up to 0.3%, the behavior of second-hand sensors was very close to each other and a minor difference was observed at strains larger than 0.8%. This is due to the strong dependency of the tunneling on the insulation thickness between two CNTs islands [36]. At longer loading times and larger strains, the distances between CNTs increased, and more noticeable differences in results were observed. However, for the most extreme conditions after 12 h loading, the deviation of the curve from its initial state is very small (about 0.4%), which can be ignored, showing the significant durability of the fabricated sensor. Another important characteristic of strain gauges is their response to periodic loading, which was investigated and presented in **Fig. 7((e) and (f))**. In this figure, which corresponds to a loading frequency of 1 Hz and a strain range of 0 to 1%, the curve of $\frac{\Delta R}{R_0}$ follows exactly the strain harmony. The phase shift between these two curves

represents the rise time of the sensor, which is shown in **Fig. 7(f)** as a magnified part of **Fig. 7(e)**. Accordingly, this time for the designed sensor is about 18 ms, indication faster response time compared to other reported sensors.

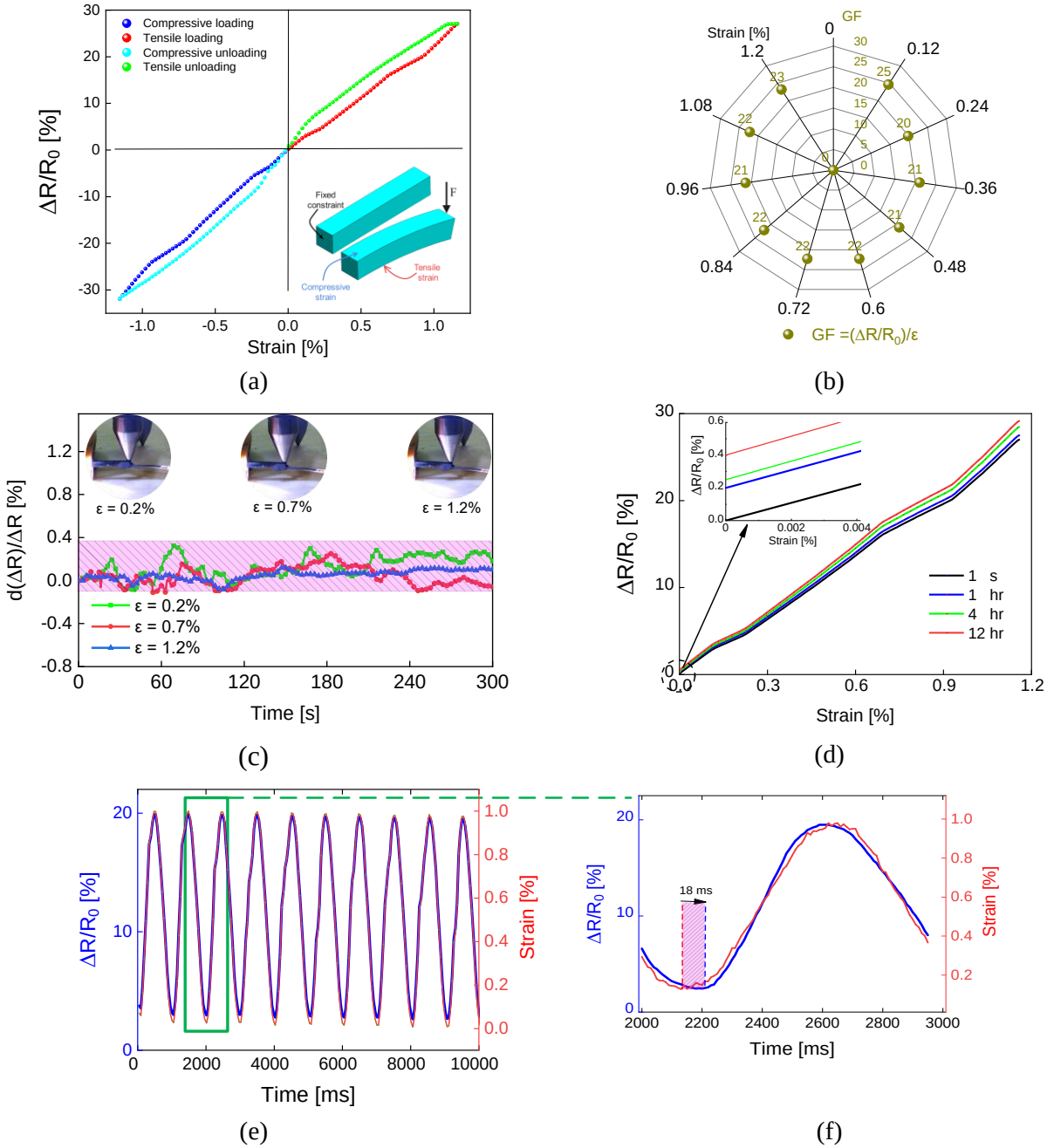

Figure 7. Results of the evaluation of electrical and electromechanical characteristics of the sensor (a), changes in ($\frac{\Delta R}{R_0}$) for the sensor under tensile and compressive strains (b), gauge factor (*GF*) at different applied strains

(c), changes in the sensor resistance under periodic loadings at a frequency of 1 Hz, ε=1%, and sensor response rise time (d), the sensor performance after continuous periodic loadings over 3000 s (e), and sensor output stability at different strains over time (f).

4. Conclusions

In this study, a two-step process was used successfully to fabricate ultrasensitive strain gauges. In the first step, the PMMA/CNTs nanocomposite was fabricated by electro-mechanically dispersion technique. In the second step, the innovative LBM/USVs methods were employed to make the surfaces of the fabricated nanocomposite conductive. The results of various evaluations of the sample surfaces and their performances as ultrasensitive strain gauges can be summarized as follows:

- The application of the USVs can arrange the placement of CNTs in such a way that the electron transmission is carried out more via the tunneling phenomenon. The USVs also help reduce the wrapping of PMMA chains around CNTs on the treated surfaces intensely.
- The fabricated sensor in the presence of the USVs at P=80 W and V=37.5 mm/s displayed the most favorable qualifications to become a sensitive strain gauge due to its extreme sensitivity. In this respect, a tunneling-based structure was created, by which better CNTs dispersion in the treated layer and the thinner PMMA barriers between CNTs were achieved.
- The ideal sample at the strain of 1.2% with a relative resistance change of 25%, approximate gauge factor of 20, negligible hysteresis, output signal changes in the range of -0.1 to +0.3, high durability, and shorter response time (~ 20 ms) presented very stunning sensory performance.

References:

[1] P. Tutak, Application of strain gauges in measurements of strain distribution in complex objects, Journal of Applied Computer Science Methods, 6 (2014).
[2] J.-u. Lee, Application of strain gauge method for investigating influence of ship shaft movement by hydrodynamic propeller forces on shaft alignment, Measurement, 121 (2018) 261-275.
[3] Y.-F. Yang, L.-Q. Tao, Y. Pang, H. Tian, Z.-Y. Ju, X.-M. Wu, Y. Yang, T.-L. Ren, An ultrasensitive strain sensor with a wide strain range based on graphene armour scales, Nanoscale, 10 (2018) 11524-11530.
[4] A.A. Basheer, Advances in the smart materials applications in the aerospace industries, Aircraft Engineering and Aerospace Technology, 92 (2020) 1027-1035.
[5] M. Fajkus, J. Nedoma, M. Pinka, P. Mec, M. Novak, S. Zabka, Deformation sensor composed of fiber Bragg grating and the strain gauge for use in civil engineering, Electro-Optical Remote Sensing XII, International Society for Optics and Photonics2018, pp. 107960T.
[6] Y.-T. Huang, S.-C. Huang, C.-C. Hsu, R.-M. Chao, T.K. Vu, Design and fabrication of single-walled carbon nanonet flexible strain sensors, Sensors, 12 (2012) 3269-3280.
[7] J. DeGraff, R. Liang, M.Q. Le, J.-F. Capsal, F. Ganet, P.-J. Cottinet, Printable low-cost and flexible carbon nanotube buckypaper motion sensors, Materials & Design, 133 (2017) 47-53.
[8] D. Lee, H.P. Hong, M.J. Lee, C.W. Park, N.K. Min, A prototype high sensitivity load cell using single walled carbon nanotube strain gauges, Sensors and Actuators A: Physical, 180 (2012) 120-126.
[9] O. Yakovenko, O. Lazarenko, L. Matzui, L. Vovchenko, M. Borovoy, P. Tesel'ko, O. Lozitsky, K. Astapovich, A. Trukhanov, S. Trukhanov, Effect of Ga content on magnetic properties of BaFe12−xGaxO19/epoxy composites, Journal of Materials Science, 55 (2020) 9385-9395.
[10] O. Yakovenko, L.Y. Matzui, L. Vovchenko, V. Oliynyk, A. Trukhanov, S. Trukhanov, M. Borovoy, P. Tesel'ko, V. Launets, O. Syvolozhskyi, Effect of magnetic fillers and their orientation on the electrodynamic properties of BaFe12-xGaxO19 (x= 0.1–1.2)—epoxy composites with carbon nanotubes within GHz range, Applied Nanoscience, 10 (2020) 4747-4752.
[11] S.A. Habib, S.A. Saafan, T.M. Meaz, M.A. Darwish, D. Zhou, M.U. Khandaker, M.A. Islam, H. Mohafez, A.V. Trukhanov, S.V. Trukhanov, Structural, Magnetic, and AC Measurements of Nanoferrites/Graphene Composites, Nanomaterials, 12 (2022) 931.
[12] A.V. Trukhanov, D.I. Tishkevich, S.V. Podgornaya, E. Kaniukov, M.A. Darwish, T.I. Zubar, A.V. Timofeev, E.L. Trukhanova, V.G. Kostishin, S.V. Trukhanov, Impact of the nanocarbon on magnetic and electrodynamic properties of the ferrite/polymer composites, Nanomaterials, 12 (2022) 868.
[13] M. Amjadi, M. Turan, C.P. Clementson, M. Sitti, Parallel microcracks-based ultrasensitive and highly stretchable strain sensors, ACS applied materials & interfaces, 8 (2016) 5618-5626.
[14] K. Parmar, M. Mahmoodi, C. Park, S.S. Park, Effect of CNT alignment on the strain sensing capability of carbon nanotube composites, Smart materials and structures, 22 (2013) 075006.
[15] S. Tong, W. Yuan, H. Liu, N. Hu, C. Zhao, Y. Zhao, Linear strain sensor made of multi-walled carbon nanotube/epoxy composite, Materials Research Express, 4 (2017) 115008.
[16] E. Roh, B.-U. Hwang, D. Kim, B.-Y. Kim, N.-E. Lee, Stretchable, transparent, ultrasensitive, and patchable strain sensor for human–machine interfaces comprising a nanohybrid of carbon nanotubes and conductive elastomers, ACS nano, 9 (2015) 6252-6261.
[17] J. Manzano-Santamaría, M. Sánchez, X. Sánchez-Romate, J. Rams, A. Ureña, Analysis of strain sensitivity under flexural load of 3D printed carbon nanotube-doped epoxy circuits, Nanotechnology, 32 (2021) 185501.
[18] A. Bsoul, M. Sultan Mohamed Ali, A. Nojeh, K. Takahata, Piezoresistive strain sensing using carbon nanotube forests suspended by Parylene-C membranes, Applied Physics Letters, 100 (2012) 213510.

[19] S. Trukhanov, A. Trukhanov, V. Turchenko, A.V. Trukhanov, E. Trukhanova, D. Tishkevich, V. Ivanov, T. Zubar, M. Salem, V. Kostishyn, Polarization origin and iron positions in indium doped barium hexaferrites, Ceramics International, 44 (2018) 290-300.
[20] V.A. Turchenko, S.V. Trukhanov, V.G.e. Kostishin, F. Damay, F. Porcher, D.S. Klygach, M.G.e. Vakhitov, L.Y.e. Matzui, O.S. Yakovenko, B. Bozzo, Impact of In3+ cations on structure and electromagnetic state of M− type hexaferrites, Journal of Energy Chemistry, 69 (2022) 667-676.
[21] S. Ryu, P. Lee, J.B. Chou, R. Xu, R. Zhao, A.J. Hart, S.-g. Kim, Fabrication of Extremely Elastic Wearable Strain Sensor Using Aligned Carbon Nanotube Fibers for Monitoring Human Motion.
[22] N. Hu, Y. Karube, M. Arai, T. Watanabe, C. Yan, Y. Li, Y. Liu, H. Fukunaga, Investigation on sensitivity of a polymer/carbon nanotube composite strain sensor, Carbon, 48 (2010) 680-687.
[23] O.A. Araromi, M.A. Graule, K.L. Dorsey, S. Castellanos, J.R. Foster, W.-H. Hsu, A.E. Passy, J.J. Vlassak, J.C. Weaver, C.J. Walsh, Ultra-sensitive and resilient compliant strain gauges for soft machines, Nature, 587 (2020) 219-224.
[24] X. Wang, J. Sparkman, J. Gou, Strain sensing of printed carbon nanotube sensors on polyurethane substrate with spray deposition modeling, Composites Communications, 3 (2017) 1-6.
[25] H. Zhao, Y. Zhang, P.D. Bradford, Q. Zhou, Q. Jia, F.-G. Yuan, Y. Zhu, Carbon nanotube yarn strain sensors, Nanotechnology, 21 (2010) 305502.
[26] T. Yamada, Y. Hayamizu, Y. Yamamoto, Y. Yomogida, A. Izadi-Najafabadi, D.N. Futaba, K. Hata, A stretchable carbon nanotube strain sensor for human-motion detection, Nature nanotechnology, 6 (2011) 296-301.
[27] Q. Fan, Z. Qin, S. Gao, Y. Wu, J. Pionteck, E. Mäder, M. Zhu, The use of a carbon nanotube layer on a polyurethane multifilament substrate for monitoring strains as large as 400%, Carbon, 50 (2012) 4085-4092.
[28] M. Abshirini, M. Charara, Y. Liu, M. Saha, M.C. Altan, 3D printing of highly stretchable strain sensors based on carbon nanotube nanocomposites, Advanced Engineering Materials, 20 (2018) 1800425.
[29] N. Lu, C. Lu, S. Yang, J. Rogers, Highly sensitive skin-mountable strain gauges based entirely on elastomers, Advanced Functional Materials, 22 (2012) 4044-4050.
[30] D.J. Cohen, D. Mitra, K. Peterson, M.M. Maharbiz, A highly elastic, capacitive strain gauge based on percolating nanotube networks, Nano letters, 12 (2012) 1821-1825.
[31] J. Lee, S. Pyo, D.S. Kwon, E. Jo, W. Kim, J. Kim, Ultrasensitive strain sensor based on separation of overlapped carbon nanotubes, Small, 15 (2019) 1805120.
[32] D. Lee, H.P. Hong, C.J. Lee, C.W. Park, N.K. Min, Microfabrication and characterization of spray-coated single-wall carbon nanotube film strain gauges, Nanotechnology, 22 (2011) 455301.
[33] A.H.A. Hoseini, M. Arjmand, U. Sundararaj, M. Trifkovic, Significance of interfacial interaction and agglomerates on electrical properties of polymer-carbon nanotube nanocomposites, Materials & Design, 125 (2017) 126-134.
[34] M. Arjmand, Electrical conductivity, electromagnetic interference shielding and dielectric properties of multi-walled carbon nanotube/polymer composites, (2014).
[35] M. Mahmoodi, Electrical, thermal, and machining behaviour of injection moulded polymeric cnt nanocomposites, (2013).
[36] N. Hu, Y. Karube, C. Yan, Z. Masuda, H. Fukunaga, Tunneling effect in a polymer/carbon nanotube nanocomposite strain sensor, Acta materialia, 56 (2008) 2929-2936.
[37] M. Almessiere, N. Algarou, Y. Slimani, A. Sadaqat, A. Baykal, A. Manikandan, S. Trukhanov, A. Trukhanov, I. Ercan, Investigation of exchange coupling and microwave properties of hard/soft (SrNi0. 02Zr0. 01Fe11. 96O19)/(CoFe2O4) x nanocomposites, Materials Today Nano, 18 (2022) 100186.
[38] M.A. Almessiere, A.V. Trukhanov, Y. Slimani, K. You, S.V. Trukhanov, E.L. Trukhanova, F. Esa, A. Sadaqat, K. Chaudhary, M. Zdorovets, Correlation between composition and electrodynamics properties

in nanocomposites based on hard/soft ferrimagnetics with strong exchange coupling, Nanomaterials, 9 (2019) 202.
[39] Y. Zare, K.Y. Rhee, A simple methodology to predict the tunneling conductivity of polymer/CNT nanocomposites by the roles of tunneling distance, interphase and CNT waviness, RSC advances, 7 (2017) 34912-34921.
[40] R. Razavi, Y. Zare, K.Y. Rhee, The roles of interphase and filler dimensions in the properties of tunneling spaces between CNT in polymer nanocomposites, Polymer Composites, 40 (2019) 801-810.
[41] Y. Zare, K.Y. Rhee, A power model to predict the electrical conductivity of CNT reinforced nanocomposites by considering interphase, networks and tunneling condition, Composites Part B: Engineering, 155 (2018) 11-18.
[42] J.-M. Zhu, Y. Zare, K.Y. Rhee, Analysis of the roles of interphase, waviness and agglomeration of CNT in the electrical conductivity and tensile modulus of polymer/CNT nanocomposites by theoretical approaches, Colloids and Surfaces A: Physicochemical and Engineering Aspects, 539 (2018) 29-36.
[43] A.K. Ghavidel, M. Zadshakoyan, M. Arjmand, G. Kiani, A novel electro-mechanical technique for efficient dispersion of carbon nanotubes in liquid media, International Journal of Mechanical Sciences, 207 (2021) 106633.
[44] A.K. Ghavidel, T. Azdast, M. Shabgard, A. Navidfar, S. Sadighikia, Improving electrical conductivity of poly methyl methacrylate by utilization of carbon nanotube and CO2 laser, Journal of applied polymer science, 132 (2015).
[45] P. Putsch, Polymer molded bodies and printed circuit board arrangement and method for the production thereof, Google Patents2011.
[46] F. Cesano, I. Rattalino, D. Demarchi, F. Bardelli, A. Sanginario, A. Gianturco, A. Veca, C. Viazzi, P. Castelli, D. Scarano, Structure and properties of metal-free conductive tracks on polyethylene/multiwalled carbon nanotube composites as obtained by laser stimulated percolation, Carbon, 61 (2013) 63-71.
[47] N. Algarou, Y. Slimani, M. Almessiere, F. Alahmari, M. Vakhitov, D. Klygach, S. Trukhanov, A. Trukhanov, A. Baykal, Magnetic and microwave properties of SrFe12O19/MCe0. 04Fe1. 96O4 (M= Cu, Ni, Mn, Co and Zn) hard/soft nanocomposites, Journal of Materials Research and Technology, 9 (2020) 5858-5870.
[48] D. Vinnik, V. Zhivulin, D. Sherstyuk, A.Y. Starikov, P. Zezyulina, S. Gudkova, D. Zherebtsov, K. Rozanov, S. Trukhanov, K. Astapovich, Ni substitution effect on the structure, magnetization, resistivity and permeability of zinc ferrites, Journal of Materials Chemistry C, 9 (2021) 5425-5436.
[49] D.I. Tishkevich, T.I. Zubar, A.L. Zhaludkevich, I.U. Razanau, T.N. Vershinina, A.A. Bondaruk, E.K. Zheleznova, M. Dong, M.Y. Hanfi, M. Sayyed, Isostatic Hot Pressed W–Cu Composites with Nanosized Grain Boundaries: Microstructure, Structure and Radiation Shielding Efficiency against Gamma Rays, Nanomaterials, 12 (2022) 1642.
[50] T.I. Zubar, T.I. Usovich, D.I. Tishkevich, O.D. Kanafyev, V.A. Fedkin, A.N. Kotelnikova, M.I. Panasyuk, A.S. Kurochka, A.V. Nuriev, A.M. Idris, Features of Galvanostatic Electrodeposition of NiFe Films with Composition Gradient: Influence of Substrate Characteristics, Nanomaterials, 12 (2022) 2926.
[51] N. Gupta, S.M. Gupta, S. Sharma, Carbon nanotubes: Synthesis, properties and engineering applications, Carbon Letters, 29 (2019) 419-447.
[52] A.K. Ghavidel, M. Zadshakoyan, M. Arjmand, Mechanical analysis of aligned carbon nanotube bundles under electric field, International Journal of Mechanical Sciences, 196 (2021) 106289.
[53] M.S. Alkuh, M.H.N. Famili, M.M.M. Shirvan, M. Moeini, The relationship between electromagnetic absorption properties and cell structure of poly (methyl methacrylate)/multi-walled carbon nanotube composite foams, Materials & Design, 100 (2016) 73-83.
[54] A. Al-Kawaz, A. Rubin, N. Badi, C. Blanck, L. Jacomine, I. Janowska, C. Pham-Huu, C. Gauthier, Tribological and mechanical investigation of acrylic-based nanocomposite coatings reinforced with PMMA-grafted-MWCNT, Materials Chemistry and Physics, 175 (2016) 206-214.

[55] Z. Spitalsky, D. Tasis, K. Papagelis, C. Galiotis, Carbon nanotube–polymer composites: chemistry, processing, mechanical and electrical properties, Progress in polymer science, 35 (2010) 357-401.
[56] F. Caiazzo, F. Curcio, G. Daurelio, F.M.C. Minutolo, Laser cutting of different polymeric plastics (PE, PP and PC) by a CO2 laser beam, Journal of Materials Processing Technology, 159 (2005) 279-285.
[57] A. Riveiro, F. Quintero, F. Lusquiños, J. Del Val, R. Comesaña, M. Boutinguiza, J. Pou, Experimental study on the CO2 laser cutting of carbon fiber reinforced plastic composite, Composites Part A: Applied Science and Manufacturing, 43 (2012) 1400-1409.
[58] A.K. Ghavidel, M. Zadshakoyan, Comprehensive study of laser cutting effects on the properties of acrylonitrile butadiene styrene, The International Journal of Advanced Manufacturing Technology, 97 (2018) 3637-3653.
[59] G. El Haber, L. Noel, C.-F. Lin, S. Gree, L. Vidal, H.-W. Zan, N. Hobeika, O. Lhost, Y. Trolez, O. Soppera, Near-Infrared Laser Direct Writing of Conductive Patterns on the Surface of Carbon Nanotube Polymer Nanocomposites, ACS Applied Materials & Interfaces, 13 (2021) 49279-49287.
[60] A.K. Ghavidel, T. Azdast, M.R. Shabgard, A. Navidfar, S.M. Shishavan, Effect of carbon nanotubes on laser cutting of multi-walled carbon nanotubes/poly methyl methacrylate nanocomposites, Optics & Laser Technology, 67 (2015) 119-124.
[61] A. Karimzad Ghavidel, M. Shabgard, H. Biglari, Microscopic and mechanical properties of semi-crystalline and amorphous polymeric parts produced by laser cutting, Journal of Applied Polymer Science, 133 (2016).
[62] A. Karimzad Ghavidel, A. Navidfar, M. Shabgard, T. Azdast, Role of CO2 laser cutting conditions on anisotropic properties of nanocomposite contain carbon nanotubes, Journal of Laser Applications, 28 (2016) 032006.
[63] S. Trukhanov, Peculiarities of magnetic phase separation in anion-deficient La0. 70Sr0. 30MnO2. 85 manganite, Physics of the Solid State, 53 (2011) 1845-1850.
[64] S. Trukhanov, Magnetic cluster state in anion-deficient La0. 70Sr0. 30MnO2. 85 manganite, Technical Physics Letters, 37 (2011) 350-353.
[65] C. Zeng, N. Hossieny, C. Zhang, B. Wang, Synthesis and processing of PMMA carbon nanotube nanocomposite foams, Polymer, 51 (2010) 655-664.
[66] A. Tomova, G. Gentile, A. Grozdanov, M. Errico, P. Paunovic, M. Avella, A. Dimitrov, Multinanosensors Based on MWCNTs and Biopolymer Matrix—Production and Characterization, Acta Physica Polonica A, (2017).
[67] W. Bauhofer, J.Z. Kovacs, A review and analysis of electrical percolation in carbon nanotube polymer composites, Composites science and technology, 69 (2009) 1486-1498.
[68] S. Abbasi, P.J. Carreau, A. Derdouri, Flow induced orientation of multiwalled carbon nanotubes in polycarbonate nanocomposites: Rheology, conductivity and mechanical properties, Polymer, 51 (2010) 922-935.
[69] K. Menzer, B. Krause, R. Boldt, B. Kretzschmar, R. Weidisch, P. Pötschke, Percolation behaviour of multiwalled carbon nanotubes of altered length and primary agglomerate morphology in melt mixed isotactic polypropylene-based composites, Composites Science and Technology, 71 (2011) 1936-1943.
[70] J. Li, P.C. Ma, W.S. Chow, C.K. To, B.Z. Tang, J.K. Kim, Correlations between percolation threshold, dispersion state, and aspect ratio of carbon nanotubes, Advanced Functional Materials, 17 (2007) 3207-3215.
[71] I. Alig, P. Pötschke, D. Lellinger, T. Skipa, S. Pegel, G.R. Kasaliwal, T. Villmow, Establishment, morphology and properties of carbon nanotube networks in polymer melts, Polymer, 53 (2012) 4-28.
[72] S. Trukhanov, I. Troyanchuk, V. Fedotova, V. Ryzhov, A. Maignan, D. Flahaut, H. Szymczak, R. Szymczak, Magnetic properties of the nonstoichiometric Sr-doped manganites, physica status solidi (b), 242 (2005) 1123-1131.

[73] S. Trukhanov, L. Lobanovski, M. Bushinsky, V. Khomchenko, V. Fedotova, I. Troyanchuk, H. Szymczak, Microstructure evolution and magnetoresistance of the A-site ordered Ba-doped manganites, Semiconductors, 41 (2007) 507-511.
[74] S. Abbasi, Rheology, properties and microstructure development of polymer/carbon nanotube composites in microinjection molding process, École Polytechnique de Montréal2009.
[75] G. Colucci, C. Beltrame, M. Giorcelli, A. Veca, C. Badini, A novel approach to obtain conductive tracks on PP/MWCNT nanocomposites by laser printing, RSC advances, 6 (2016) 28522-28531.
[76] C.J. Long, N.D. Orloff, K.A. Twedt, T. Lam, F. Vargas-Lara, M. Zhao, B. Natarajan, K.C. Scott, E. Marksz, T. Nguyen, Giant surface conductivity enhancement in a carbon nanotube composite by ultraviolet light exposure, ACS applied materials & interfaces, 8 (2016) 23230-23235.
[77] E. Padovano, M. Bonelli, A. Veca, E. De Meo, C. Badini, Effect of long-term mechanical cycling and laser surface treatment on piezoresistive properties of SEBS-CNTs composites, Reactive and Functional Polymers, 152 (2020) 104601.
[78] A. Caradonna, C. Badini, E. Padovano, A. Veca, E. De Meo, M. Pietroluongo, Laser treatments for improving electrical conductivity and piezoresistive behavior of polymer–carbon nanofiller composites, Micromachines, 10 (2019) 63.
[79] F. Cesano, M.J. Uddin, A. Damin, D. Scarano, Multifunctional Conductive Paths Obtained by Laser Processing of Non-Conductive Carbon Nanotube/Polypropylene Composites, Nanomaterials, 11 (2021) 604.
[80] J.-s. Wang, R.S. Porter, On the viscosity-temperature behavior of polymer melts, Rheologica acta, 34 (1995) 496-503.
[81] G.C. Berry, T.G. Fox, The viscosity of polymers and their concentrated solutions, Fortschritte der Hochpolymeren-Forschung, Springer1968, pp. 261-357.
[82] N. Kedir, J.A. Hernandez, B.H. Lim, J. Gao, X. Zhai, Y. Nie, M.N. Issahaq, T.N. Tallman, W.W. Chen, Effect of laser irradiation time on the surface characteristics of a carbon fiber composite, Journal of Laser Applications, 33 (2021) 042034.
[83] M. Moradi, O. Mehrabi, T. Azdast, K.Y. Benyounis, Enhancement of low power CO2 laser cutting process for injection molded polycarbonate, Optics & Laser Technology, 96 (2017) 208-218.
[84] E. Haddadi, M. Moradi, A.K. Ghavidel, A.K. Ghavidel, S. Meiabadi, Experimental and parametric evaluation of cut quality characteristics in CO2 laser cutting of polystyrene, Optik, 184 (2019) 103-114.
[85] H. Xu, J. Hu, Study of polymer matrix degradation behavior in CFRP short pulsed laser processing, Polymers, 8 (2016) 299.
[86] D. Baskaran, J.W. Mays, M.S. Bratcher, Noncovalent and nonspecific molecular interactions of polymers with multiwalled carbon nanotubes, Chemistry of Materials, 17 (2005) 3389-3397.
[87] L. He, S.-C. Tjong, Carbon nanotube/epoxy resin composite: correlation between state of nanotube dispersion and Zener tunneling parameters, Synthetic Metals, 162 (2012) 2277-2281.
[88] J. Doh, S.-I. Park, Q. Yang, N. Raghavan, The effect of carbon nanotube chirality on the electrical conductivity of polymer nanocomposites considering tunneling resistance, Nanotechnology, 30 (2019) 465701.
[89] M. Amjadi, K.U. Kyung, I. Park, M. Sitti, Stretchable, skin-mountable, and wearable strain sensors and their potential applications: a review, Advanced Functional Materials, 26 (2016) 1678-1698.
[90] U.-H. Shin, D.-W. Jeong, S.-M. Park, S.-H. Kim, H.W. Lee, J.-M. Kim, Highly stretchable conductors and piezocapacitive strain gauges based on simple contact-transfer patterning of carbon nanotube forests, Carbon, 80 (2014) 396-404.
[91] K.K. Talamadupula, G.D. Seidel, Statistical Analysis of Effective Piezoresistivity of Carbon Nanotube Reinforced Polymer Nanocomposites from Electron Tunneling Effects, AIAA Scitech 2020 Forum2020, pp. 2259.

[92] W. Bao, S. Meguid, Z. Zhu, Y. Pan, G. Weng, Effect of carbon nanotube geometry upon tunneling assisted electrical network in nanocomposites, Journal of Applied Physics, 113 (2013) 234313.
[93] C. Gau, C.-Y. Kuo, H. Ko, Electron tunneling in carbon nanotube composites, Nanotechnology, 20 (2009) 395705.
[94] U. Heckmann, R. Bandorf, H. Gerdes, M. Lübke, S. Schnabel, G. Bräuer, New materials for sputtered strain gauges, Procedia Chemistry, 1 (2009) 64-67.
[95] M. Gamil, O. Tabata, K. Nakamura, A.M. El-Bab, A.A. El-Moneim, Investigation of a new high sensitive micro-electromechanical strain gauge sensor based on graphene piezoresistivity, Key Engineering Materials, Trans Tech Publ2014, pp. 207-210.
[96] M. Yee, A.M. Souza, T.S. Valera, N.R. Demarquette, Stress relaxation behavior of PMMA/PS polymer blends, Rheologica acta, 48 (2009) 527-541.
[97] F. Meng, R.H. Pritchard, E.M. Terentjev, Stress relaxation, dynamics, and plasticity of transient polymer networks, Macromolecules, 49 (2016) 2843-2852.
[98] A. Sanli, A. Benchirouf, C. Müller, O. Kanoun, Piezoresistive performance characterization of strain sensitive multi-walled carbon nanotube-epoxy nanocomposites, Sensors and Actuators A: Physical, 254 (2017) 61-68.
[99] Y. Zare, K.Y. Rhee, Calculation of tunneling distance in carbon nanotubes nanocomposites: effect of carbon nanotube properties, interphase and networks, Journal of Materials Science, 55 (2020) 5471-5480.